DOI: 10.21062/mft.2026.041 © 2026 Manufacturing Technology. All rights reserved. http://www.journalmt.com

Design and Analysis of High-Precision Hydraulic Press Frame for Aviation based on Finite Element Method

Lu Dong (0009-0002-8829-8667), Yaoming Fu (0009-0005-6262-4067)*, Jie Pang (0009-0000-6734-8560), Rui Nie (0009-0004-4319-9264), Zehua Hua (0009-0006-3655-5747)
Civil Aviation Flight University of China, Guanghan Sichuan, 618300, China. *E-mail of the corresponding author: z7fu65@163.com

As the core equipment for compression molding of aerospace products, the strength, stiffness, and dynamic stability of the four-column frame of the aviation high-precision hydraulic press directly determine product molding accuracy and production safety. This study optimizes the frame structure and conducts multi-condition finite element analysis using ANSYS. The initial stress concentration is identified by static strength analysis. After improvement, the maximum stress in pre-tightening and working states decreases by 41.87 % and 66.20 % respectively. Modal analysis shows that the deformation of the first ten modes is uniform. It is confirmed that the columns are the weak link, and its inner slope is optimized to obtain optimal load-bearing. Under 5mm eccentric load, the maximum stress does not exceed the material yield limit, and deformation is ≤1.06 mm. The improved structure effectively solves the problem of stress concentration, improves the ability to resist eccentric load and dynamic stability, providing a structural guarantee for reliable operation.

Keywords: Aviation high-precision hydraulic press, Frame structure, Finite element analysis, Static strength, Modal analysis, Eccentric load condition, Structural optimization

1 Introduction

In the aerospace manufacturing, the compression molding of key aircraft components (such as engine blades, aerospace structural parts, and more) puts forward strict requirements on equipment accuracy and stability [1-3]. As a core equipment to realize this high-difficulty molding, the frame of aviation high-precision hydraulic presses (as the main load-bearing component) must maintain minimal deformation under heavy load and complex dynamic conditions, as well as high fatigue resistance and eccentric load resistance [4-5].

The four-column frame is widely used in hydraulic press design due to its simple structure and uniform load-bearing characteristics [6]. However, in high-precision aviation applications, traditional frames often have problems such as stress concentration, excessive dynamic vibration, and insufficient adaptability to eccentric loads [7]. During the molding process of aerospace products, slight deformation or vibration of the frame may lead to deviations in the dimensional accuracy of components [8-9]. The frequent of eccentric load is more likely to cause structural fatigue damage, seriously affecting production efficiency and product quality [10-11]. Therefore, it is of crucial engineering significance to meet the strict operational requirements of high-precision hydraulic presses in aviation through rigorous optimization design and comprehensive finite element analysis. This systematic approach is essential for ensuring the structural integrity required to maintain dimensional fidelity of critical aerospace components.

Some studies first focused on static strength simulation of integrally cast frames and then investigated pre-stressed winding structures. Current work is limited to individual static and modal analysis, without comprehensive working condition check for eccentric loads or parameter optimization of column inner wall inclination [1, 3, 6]. In addition, there are few studies proposing specialized framework optimization for aerospace-oriented press machines to achieve lightweight and high-precision forming. Some studies have focused on the overall stiffness of heavy-duty forging hydraulic presses, with little research on four column prestressed frames used for high-precision forming in aerospace. The existing optimization only modifies the beam structure and rarely combines the parameter adjustment of the inclined surface of the column inner wall with node verification under multi-directional eccentric loads [2, 4, 9].

In this work, the frame of high-precision hydraulic press for aviation is established as the main object. Then a rigorous tripartite assessment is conducted through an integrated digital workflow combining Solid Edge modeling with ANSYS simulation. This study systematically explores the performance boundaries of structures, with a particular focus on

their static yield strength, dynamic vibration characteristics, and elasticity under asymmetric eccentric load disturbances. Structural weak links are determined first; then structural design and key parameters are optimized, and finally the reliability of the improved frame under various working conditions is verified. The quantitative insights and optimization strategies provide a validated engineering reference, providing essential theoretical guidance for the development of next-generation aviation hydraulic presses. Ultimately, this study facilitated a shift in manufacturing standards, greatly improving the forming accuracy and dynamic stability required for reliable production of complex aerospace structures.

2 Materials and methods

2.1 Fatigue strength analysis of prestressed frames

The principle of the wire-wound prestressed frame is to first separate the upper and lower semi-circular beams and columns, and then use high-strength steel wires (preload members) to wind the columns and upper/lower beams (preloaded members) layer-by-layer into a composite structure. Before bearing load, the frame is subjected to preload. During operation, the stress directions caused by the prestress and working load are opposite, thereby offsetting all or most of the stress caused by the working load on the frame (the total preload applied is generally 1.5 times the maximum working load or higher). Therefore, the load-bearing capacity of the entire structure is significantly improved.

After preloading, the equivalent stresses on the prestressed frame and the non-prestressed frame are respectively [11] as follows:

$$\begin{cases} \sigma_{D_r} = -\dfrac{\dfrac{\sigma_1}{2}\left(\dfrac{C}{1+C}\right)}{1-\dfrac{\dfrac{\sigma_1}{2}\left(2\eta+\dfrac{C}{1+C}\right)}{\sigma_b}} \\ \sigma_{D_i} = \dfrac{\dfrac{\sigma_2}{2}}{1-\dfrac{\dfrac{\sigma_2}{2}}{\sigma_b}} \end{cases} \quad (1)$$

Where:

σ_1 …The average stress caused by the working load F on the steel wire layer;

σ_2 …The allowable stress of the column;

σ_b …The ultimate strength of the steel wire material;

n…The safety factor;

η …The preload coefficient;

C …The stiffness ratio of the steel wire to the column.

Key parameters are calculated as follows [11]:

$$\begin{cases} \sigma_1 = \dfrac{\sigma_b}{n\left(\eta+\dfrac{C}{1+C}\right)} \\ \sigma_2 = \dfrac{\sigma_b}{n} \\ C = \dfrac{A_W E_W}{A_C E_C} \end{cases} \quad (2)$$

Where:

E_w, A_w …The elastic modulus and cross-sectional area of the steel wire, respectively;

E_C, A_C …The elastic modulus and cross-sectional area of the column material respectively.

Due to $E_W \approx E_C$, so $C \approx \dfrac{A_W}{A_C}$. Substituting σ_1 and σ_2 into Formula (1):

$$\begin{cases} \sigma_{D_r} = -\dfrac{\left(\dfrac{C}{1+C}\right)\sigma_b}{2\eta(n-1)+(2n-1)\dfrac{C}{1+C}} \\ \sigma_{D_i} = \dfrac{\sigma_b}{2n-1} \end{cases} \quad (3)$$

Then, the ratio of the equivalent stress borne by the prestressed frame to that of the non-prestressed frame during operation is:

$$K = \frac{|\sigma_{D_r}|}{\sigma_{D_i}} = \left|\frac{(2n-1)C}{(2n-1)C+2\eta(n-1)(1+C)}\right| \quad (4)$$

Generally, $n > 1$, $\eta > 1$, and $0 < C < 1$. Therefore, $0 < K < 1$, indicating that the stress borne by the prestressed frame is significantly reduced compared with the non-prestressed frame. In addition, $\sigma_{Dr} < 0$, meaning the frame is always subjected to compressive stress.

2.2 Improved design of 3D model

2.2.1 Initial model of the frame

This hydraulic press adopts a four-column frame. After simplifying some components and deleting some unnecessary threaded holes and unimportant chamfers in Solid Edge software, the designed 3D model is imported into ANSYS software to obtain the preliminary frame model, as shown in Fig. 1. It is mainly composed of (1) upper semicircular beam, (2) lower semicircular beam, (3) four columns, (4) fixed workbench, and (5) base, where the columns adopt a slotted rectangular structure. The fuselage material is the upper semicircular beam using ZG310-570H cast steel, and other components select 45- steel. The steel

strip composed of flat steel wires is 65Mn high-strength spring steel strip with a tensile limit of greater than 1800 MPa to ensure high tensile. The dimensional specifications of the frame are established as follows: a column height of 7710 mm and a semicircular beam radius of 1740 mm. The structure incorporates a flat steel wire layer with a thickness of 78 mm, and the spacing between the two semicircular beams is 2480 mm.

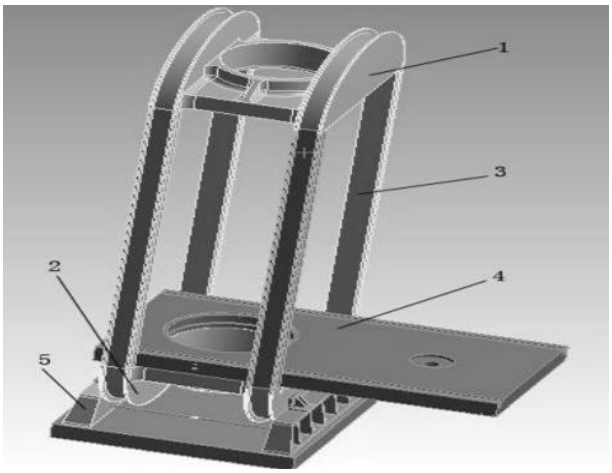


Fig. 1 *The original 3D model of the frame*

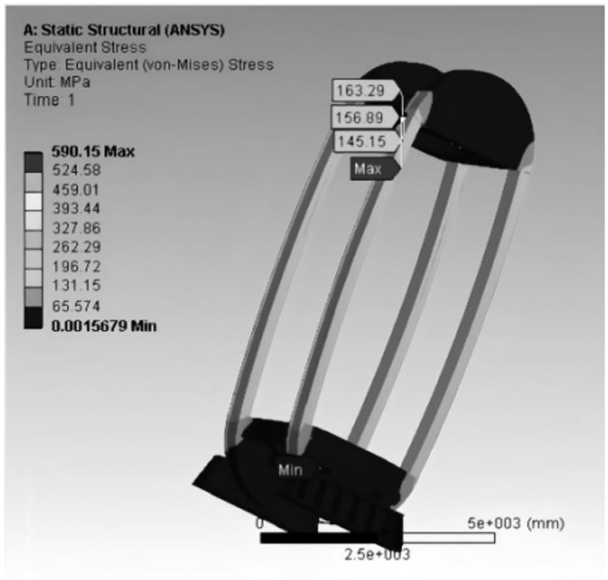
Where:
1…Upper-semicircular beam;
2…Lower-semicircular beam;
3…Column;
4…Fixed workbench;
5…Base.

2.2.2 Static strength analysis of the initial model

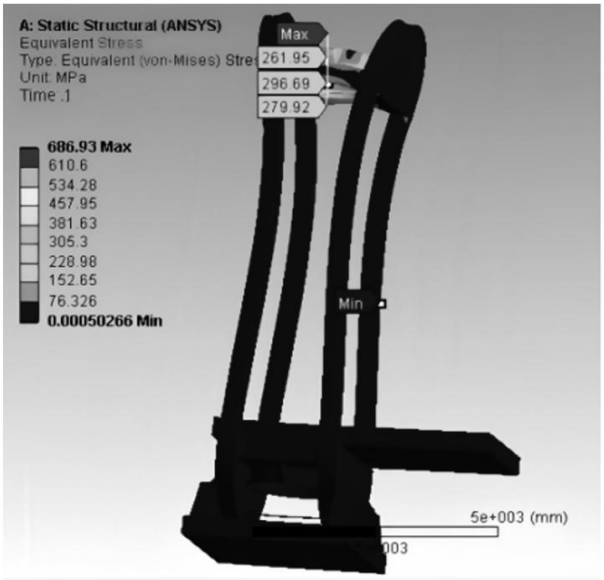
In actual work, the rated working load is F=45 MN, and the pre-tightening coefficient η is set to 1.2. Therefore, the pre-tightening force Fc applied to the frame is F×η=54 MN. According to the actual winding situation, a pre-tightening force of 27 MN is applied to each of the four arc surfaces where the semicircular beam contacts the flat steel wire.

The mechanical stress distribution of the frame in its pre-tightening configuration and under full working load is determined through rigorous finite element analysis using ANSYS software. The simulation results for the pre-tightening state (the stress nephogram in Fig. 2(a)) reveal a highly non-uniform stress field. The critical peak equivalent stress of 590.15 MPa has been determined and clearly located at the geometric interface connecting the supporting column and the upper semi-circular beam.

Fig. 2(b) is the stress nephogram of the frame in the working state. The resulting stress field shows significant non-uniformity across the structure. The maximum equivalent stress recorded is 686.93 MPa, mainly concentrated at the structural interface connecting the upper semi-circular beam and the hydraulic cylinder component.



(a) Stress nephogram in pre-tightening state



(b) Stress nephogram in working state

Fig. 2 *Stress diagram of the preliminary designed frame model*

Based on the finite element simulation results, the mechanical behaviors of the frame can be drawn as follows:

- (1) The peak equivalent stress values recorded in the pre-tightening and rated working states remain strictly below the yield strength threshold of the frame material. Consequently, the fuselage is theoretically secure against immediate plastic deformation or catastrophic structural failure under these specific loading conditions;

- (2) The stress magnitude under the working load significantly exceeds that of the pre-tightening phase. This escalation highlights a necessity for targeted design enhancements to bolster the safety factor and operational robustness during active compression cycles;
- (3) Both load cases show highly non-uniform stress distributions. This heterogeneity creates localized stress concentration zones, where the maximum stress value is dangerously high relative to the average, making the structure susceptible to potential fatigue problems and reducing long-term reliability;
- (4) The analysis identifies the junction of the upper semicircular beam as the locus of maximum stress accumulation. This finding designates the upper semicircular beam as the most vulnerable component within the assembly, requiring a comprehensive structural redesign to mitigate failure risks and ensure durability.

2.2.3 Improved frame model

The main model of the frame is significantly improved as evidenced by above results and analysis: ① Two connecting plates are added between the two upper semi-circular beams for reinforcement and safety; ② a support is added at the workbench to eliminate stress concentration; ③ the material of the entire frame is changed to 35CrMo alloy steel with a yield strength of 835 MPa, guaranteeing high performance in strength, impact toughness and fatigue resistance (The material selection refers to national standards and relevant literatures). Fig. 3 shows the 3D model diagram of the improved frame.

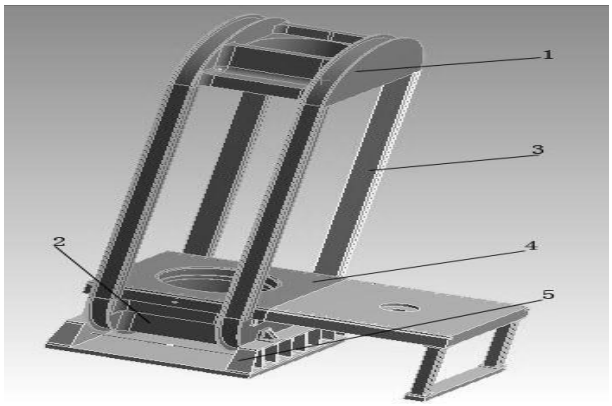


Fig. 3 *The improved model of the frame*

Where:
1…Upper semicircular beam;
2…Lower semicircular beam;
3…Column;
4…Fixed workbench;
5…Base.

2.2.4 Static strength analysis after improved design

ANSYS static analysis is performed again on the improved frame model. Fig. 4(a) is the stress distribution diagram in the pre-tightening state. The maximum stress is 343.04 MPa, and the location is transferred from the junction of the upper semicircular beam and the column to the column, eliminating the stress concentration at the upper semicircular beam.

Fig. 4(b) is the stress distribution diagram in the working state. Under the rated working load, the frame has a peak stress of 232.16 Mpa. This maximum clearly appears at the load-transferring boundary between the upper semicircular beam and the oil cylinder.



(a) Stress nephogram in pre-tightening state (b) Stress nephogram in working state

Fig. 4 *Stress diagram of the improved frame model*

The quantitative evaluation compared with the initial model shows that the maximum stress experienced by the optimized design framework has been significantly improved. The specific reduction of peak stress amplitude under the two critical working conditions simulated is calculated as follows:

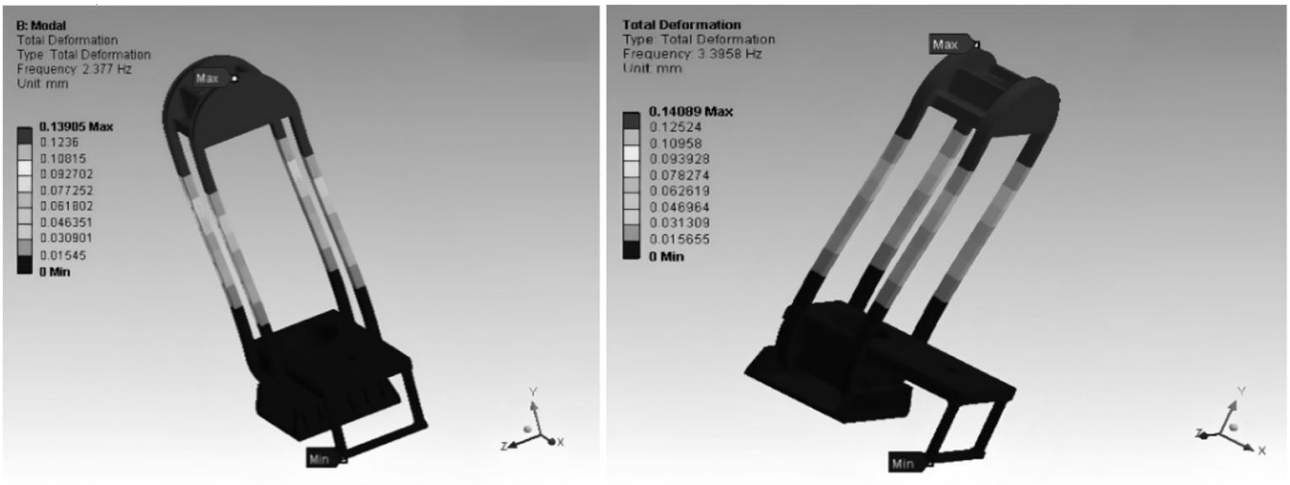
$$\text{Pre-tightening state: } (590.15-343.04)/590.15=41.87\%$$
$$\text{Working state: } (686.93-232.16)/686.93=66.20\% \quad (5)$$

This indicates that the improved design of this frame can effectively reduce stress concentration, especially in the working state. It can achieve uniform stress distribution and improve the static load-bearing capacity of the entire structure. Meanwhile, the application of 35CrMo steel (yield strength: 835 MPa) can effectively improve the strength margin and safety factor of this model. Therefore, these columns can reduce size and weight, in line with the aerospace lightweight and high-precision design goals.

2.3 Modal analysis of the improved frame structure

For this frame architecture, the overall performance evaluation requires a study that goes beyond simple static strength parameters and rigorously characterize the dynamic behaviors and vibrational stability of the system [12]. The engineering application background of this frame is the high-precision compression molding of aerospace products. Therefore, the requirements for its structural stability are extremely high. Modal analysis can predict the vibration response of the frame under dynamic conditions, and the results can identify potential vibration risks [13-14]. Accordingly, the advanced simulation capabilities of ANSYS are used for modal analysis of the optimized frame. This step is crucial for evaluating the resonant behavior of the system under dynamic loading constraints.

The first few natural frequencies of the structure are relatively low and have a significant impact on the vibration characteristics of the structure. Therefore, the first ten orders of modes are selected for analysis. Fig. 5 shows the mode shape diagrams from the modal analysis. (To save space, only the images of the first two order modal analysis are presented.)



(a) First-order mode shape (b) Second-order mode shape

Fig. 5 *Modal analysis diagrams of the improved frame structure model*

Due to the fact that the vibration mode of the subsequent modal analysis is mainly dominated by the vibration of the column, the changes in frequency and displacement deformation are not significant. Therefore, they are not shown in the figure. Table 1 shows the data results of the modal analysis.

The dynamic analysis results of the improved frame model can be obtained as follows:

- (1) The overall deformation of the frame is small, and the deformation nephogram is relatively uniformly distributed. This indicates that the improved frame structure has sufficient overall stiffness and meets the requirements;
- (2) In the extracted modes, the fifth-order frequency corresponds to the maximum deformation magnitude. This vibrational response is mainly concentrated in the mid-section of the column. The deformation profile has a classic bowing effect, where the amplitude reaches its zenith in the center and gradually diminishes toward the terminal anchor points;

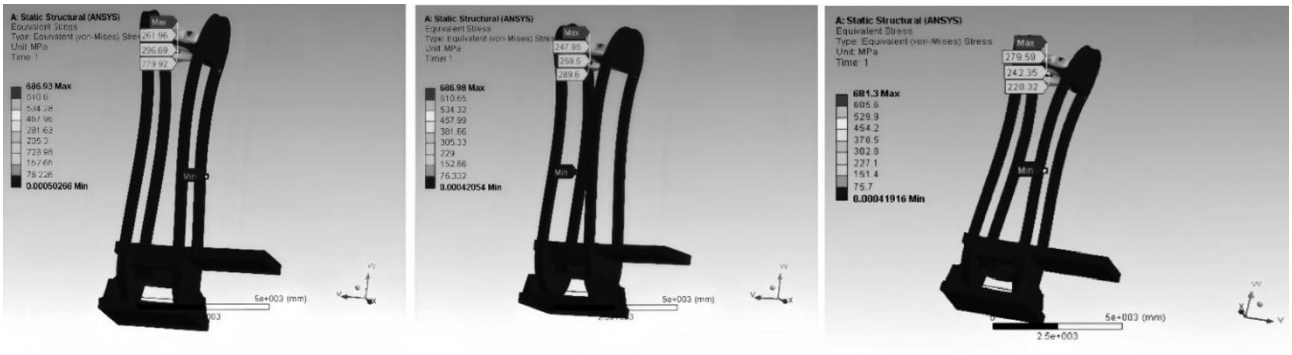
- (3) The mode shapes of the overall frame structure are basically the vibration of the columns, and the maximum vibration deformation basically appears in the column section. This indicates that the columns are the relatively weak part of the entire structure.

Tab. 1 *Modal analysis results of the improved frame model*

Order	Frequency (Hz)	Maximum Displacement (mm)	Location of Maximum Displacement
1	2.38	0.13905	Top of the top beam
2	3.40	0.14089	Top of the top beam
3	6.05	0.21121	Junction of column and top beam
4	22.57	0.46189	Middle section of the column
5	22.59	0.48965	Middle section of the column
6	23.12	0.34874	Middle section of the column
7	23.52	0.34765	Middle section of the column
8	26.10	0.31358	Middle section of the column
9	26.11	0.21755	Middle section of the column
10	26.42	0.15601	Middle section of the column

2.4 Slope design of the inner side of the columns

From the above modal analysis, the columns are the weakest part of the entire frame structure, which guides subsequent inner slope optimization. In fact, the load-bearing capacity of the columns is different when different inclined planes are adopted for the inner side of the columns. To find the optimal slope of the columns in this design, three typical vertical surfaces (i.e., slopes of 0°, 1.5°, and 3°) are selected for comparative analysis. Static analysis of these three vertical surfaces is carried out based on ANSYS. The results are shown in Fig.6 (To save space, only the stress nephograms under three inclination conditions are presented.)



(a) Stress nephogram when slope is 0° (b) Stress nephogram when slope is 1.5° (c) Stress nephogram when slope is 3°

Fig. 6 *Comparison diagram of mechanical analysis results of the frame under working conditions with three different slopes on the inner side of the columns*

Tab. 2 *Comparison of strength analysis data of three frames under working load*

Inner side slope	Maximum stress (MPa)	Maximum deformation (mm)
0° (flat surface)	261.95	4.042
1.5° inclined surface	247.95	4.0176
3° inclined surface	279.59	4.044

As shown in Table 2, when the inner side of the column adopts a 1.5° inclined surface, the entire frame is the strongest load-bearing capacity. At this time, the stress and displacement on the column structure are the smallest. Therefore, the inner side of the frame column is finally designed to be a 1.5° inclined surface.

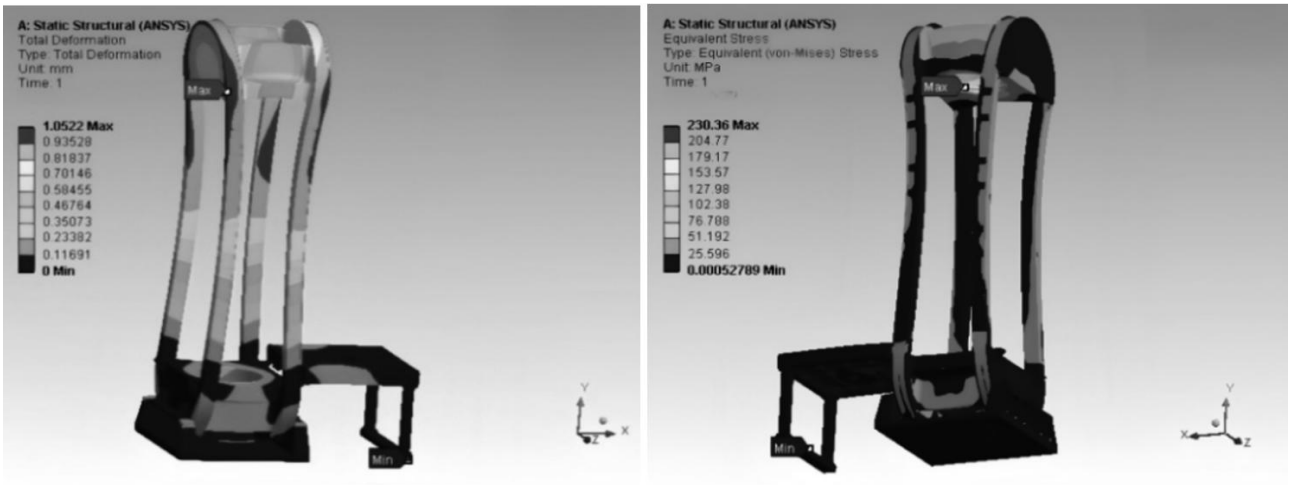
This can improve the load-bearing of column structures and improve the weak structure of the system.

3 Results and analysis

To verify the rationality of this design, considering using the stress state that is prone to failure in actual work for verification. Due to the common phenomenon of eccentric load on the frame during the working process, the load distribution on various components of the frame will be uneven due to the misalignment between the load line and the structural center of mass (or load-bearing center). This results in stress concentration on the frame and ultimately lead to fatigue damage [15]. Therefore, several typical eccentric load conditions are used to verify based on ANSYS software, with an eccentricity of 5mm. Due to the eccentric application of load on the frame structure, the frame will bear additional moments in addition to the load. The load and constraint conditions are reset in ANSYS software.

3.1 Applying positive symmetric eccentric load in X direction

As shown in Fig. 7, the maximum structural deformation is quantified at 1.0522 mm, manifesting specifically at the lower extremity of the semicircular beam. At the same time, the peak stress magnitude reaches 230.36 MPa, with the stress concentration localized at the functional interface between the semicircular beam and the hydraulic cylinder [16].

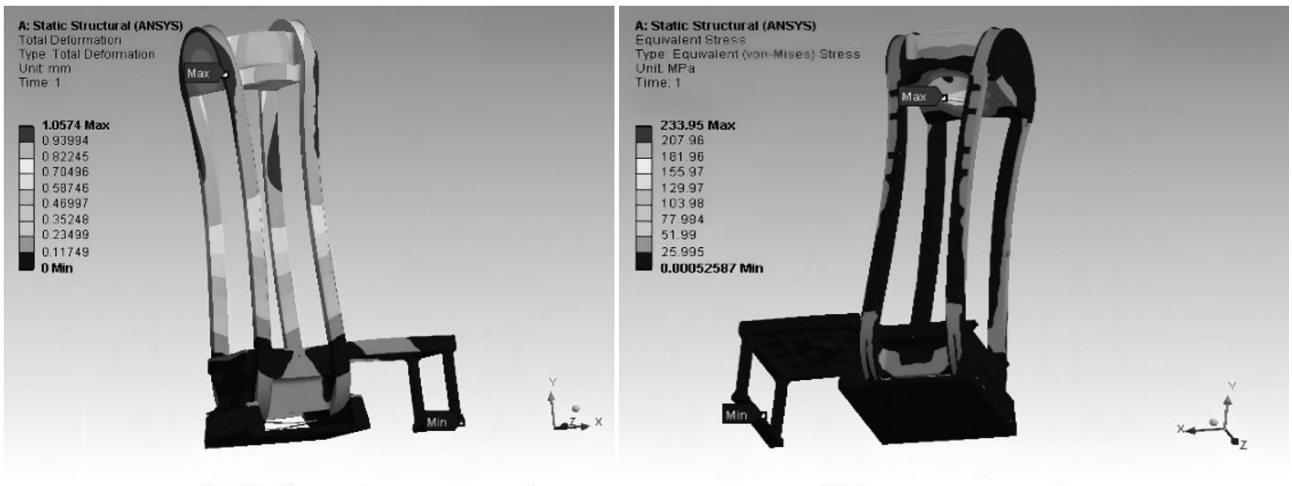


(a) Deformation contour plot (b) Stress contour plot

Fig. 7 *Static analysis results under positive symmetric eccentric loading in the X-direction*

3.2 Applying inclined symmetric eccentric load in X direction

Simulation data shows that the maximum displacement limit of the frame is 1.0574mm, occurring at the lower part of the semi-circular beam [17]. Regarding the stress field, a maximum value of 233.95 MPa is observed. This is spatially confined to the critical contact boundary separating the semicircular beam from the working oil cylinder.

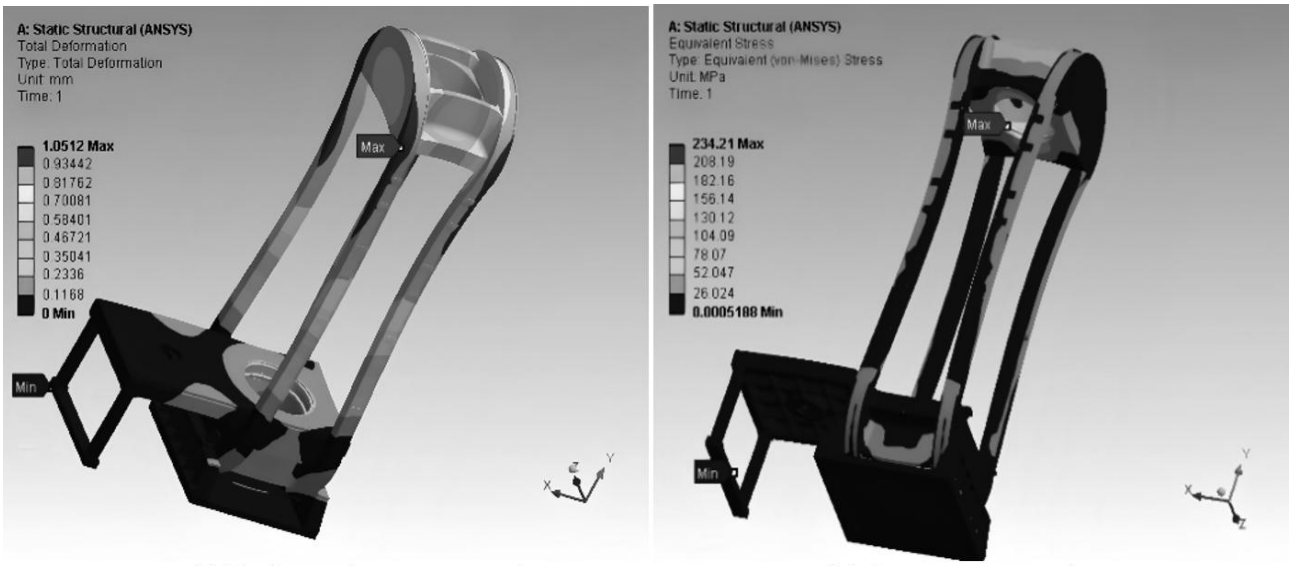


(a) Deformation contour plot (b) Stress contour plot

Fig. 8 *Static analysis results under inclined symmetric eccentric loading in the X-direction*

3.3 Applying positive symmetric eccentric load in Z direction

As shown in Fig. 9, Quantitative analysis confirms that the frame structure maintains a maximum deformation of 1.0512mm at the lower end of the semicircular beam. In addition, the analysis determines a peak equivalent stress of 234.21MPa. It is precisely concentrated at the load-bearing junction where the semi-circular beam interacts with the active oil cylinder mechanism.

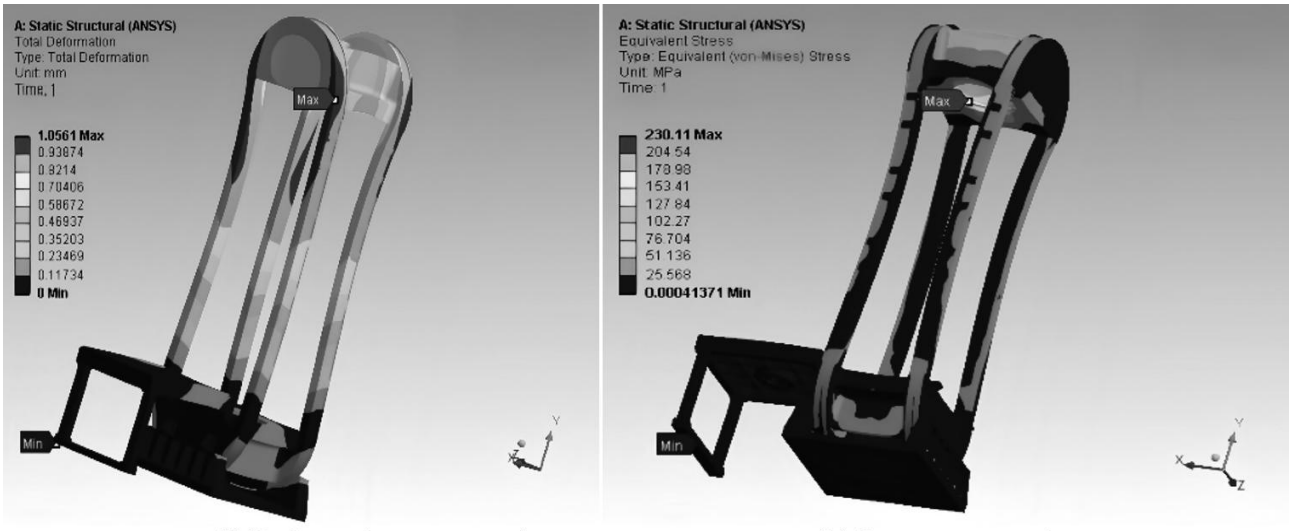


(a) Deformation contour plot (b) Stress contour plot

Fig. 9 *Static analysis results under positive symmetric eccentric loading in the Z-direction*

3.4 Applying inclined symmetric eccentric load in Z direction

As shown in Fig. 10, the examination indicates that the maximum deformation of the frame structure reaches 1.0561 mm, manifesting at the lower extremity of the semicircular beam. At the same time, the maximum recorded stress is 230.11 MPa, which is spatially limited to the contact interface between the semi-circular beam and the working cylinder.

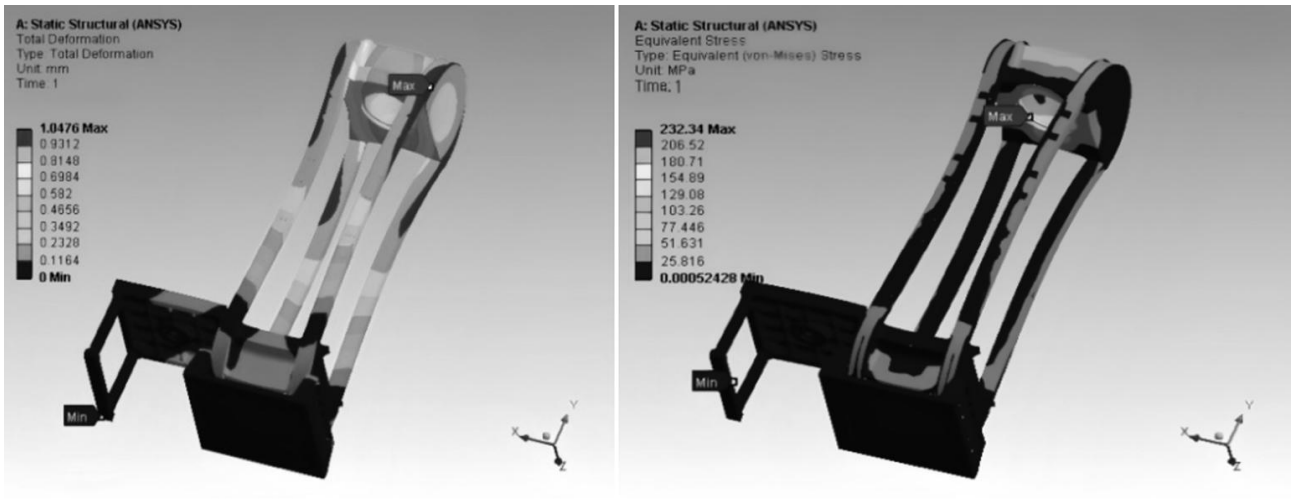


(a) Deformation contour plot (b) Stress contour plot

Fig. 10 *Static analysis results under inclined symmetric eccentric loading in the Z-direction*

3.5 Applying 45° positive symmetric eccentric load in X-Z direction

As shown in Fig. 11, the structure undergoes a peak deformation of 1.0476 mm at the inferior margin of the semi-circular beam. Future analysis identifies a maximum stress magnitude of 232.34 MPa, which is concentrated at the structural junction between the semicircular beam and the active oil cylinder.

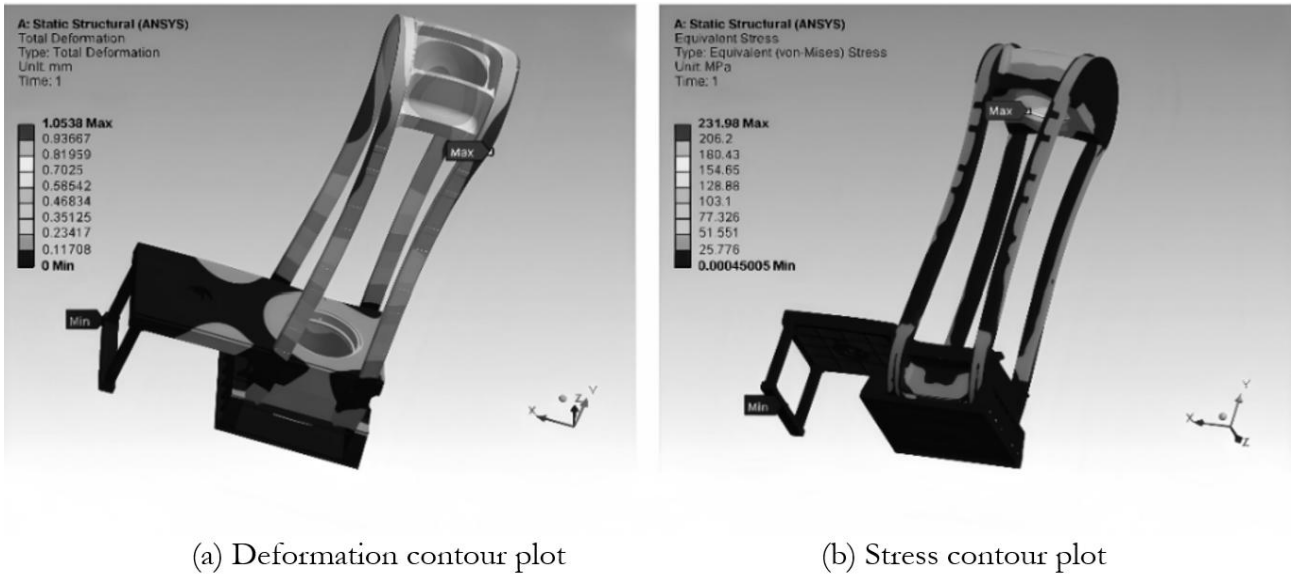


(a) Deformation contour plot (b) Stress contour plot

Fig. 11 *Static analysis results under 45° positive symmetric eccentric loading in the X-Z direction*

3.6 Applying 45° inclined symmetric eccentric load in X-Z direction

The visual data confirms that the maximum structural displacement of the system is 1.0538 mm at the lower end of the semi-circular beam. In terms of load distribution, the maximum equivalent stress is determined to be 231.98 MPa. It appears precisely at the critical contact point between the semicircular beam and the hydraulic cylinder.



(a) Deformation contour plot (b) Stress contour plot

Fig. 12 *Static analysis results under 45° inclined symmetric eccentric loading in the X-Z direction*

3.7 Simulation experiment results

Under several typical eccentric load states, the static analysis results of the frame structure are shown in the Table 3.

Based on the quantitative data in Table 3, it is evident that under all simulated eccentric loading conditions, the frame maintains robust structural integrity. The analysis confirms that the maximum stress experienced by the frame remains consistently below the yield strength threshold of the material. In addition, the structural stiffness is maintained because the maximum deformation value never exceeds the established stiffness limit of the constituent materials. That is, the strength and stiffness of the frame are within the safe range even under eccentric load conditions [18]. Therefore, the improved frame structure is reasonable and fully meets the working requirements.

All six eccentric loading cases include the X, Z and X-Z 45° directions, and they are based on typical actual fault conditions. Therefore, the analysis results are adaptable to complex eccentric working conditions in aerospace production.

Tab. 3 *Static analysis results of the frame under eccentric load states*

Eccentric Load Condition	Maximum Stress (MPa)	Maximum Deformation (mm)
X-direction positive symmetric	230.36	1.0522
X-direction inclined symmetric	233.95	1.0574
Z-direction positive symmetric	234.21	1.0512
Z-direction inclined symmetric	230.11	1.0561
X-Z 45° positive symmetric	232.34	1.0476
X-Z 45° inclined symmetric	231.98	1.0538

4 Conclusions

The frame structure is improved by multi-condition finite element analysis using ANSYS. The conclusions are drawn as follows:

- (1) Aiming at the stress concentration problem in the initial model of the aviation high-precision hydraulic press frame, the load-bearing capacity of the frame is significantly improved by adding connecting plates to reinforce the upper semicircular beam. Therefore, the support structure of the workbench is optimized to adjust the material selection (the material of the entire frame is 35CrMo). After improvement, the maximum stress of the model was reduced by 41.87% and 66.20% in the pre tensioned and working states, respectively. This can effectively avoid local stress concentration and greatly improve the safety and reliability of the structure. The improved design complies with the requirements of lightweight and high-precision in aerospace equipment;
- (2) A systematic modal analysis was conducted on the optimized frame, successfully elucidating the natural frequencies and mode shape characteristics for the first ten vibration orders. The simulation results demonstrate that the global deformation distribution is relatively uniform and contains a rational magnitude range. This empirically verifies that the dynamic stability of the structure meets the strict operating standards of high-precision hydraulic presses in aviation. It is crucial that the analysis indicates that the maximum vibration deformation in these modes is always limited to the center span of the column, thereby identifying the column structure as a critical weak link within the component;
- (3) Comparing the rigorous static performance of inner column slopes at 0°, 1.5°, and 3°, the 1.5° configuration is determined as the optimal parameter. This optimization plays a crucial role in strengthening the column, which is the limiting factor in the integrity of the frame. The implementation of this slope significantly improves the bearing capacity while minimizing stress distribution and deformation levels. Therefore, the overall stiffness and deformation resistance of the frame are enhanced. This ensures full compliance with the strict requirements of structural stability om high-precision aviation compression molding;
- (4) Under the common eccentric load in the actual operation of aviation hydraulic presses, the mechanical response of the frame under positive symmetric/inclined symmetric eccentric loads (eccentricity of 5mm) in X-direction, Z-direction, and X-Z 45° direction is systematically analyzed. Under all eccentric load states, the maximum stress of the frame does not exceed the material yield limit, and the maximum deformation is controlled within 1.06mm. Therefore, the improved frame has high eccentric load resistance and can adapt to the working requirements under complex conditions.

Through the complete process of 3D modeling, static analysis, modal analysis, and eccentric load condition verification, a relatively complete design and finite element analysis method for high-precision hydraulic press frames in aviation has been developed. The results can provide reliable theoretical data and technical support for actual installation

and manufacture of the frame. They have important practical value for improving the compression molding accuracy of aerospace products and the operational reliability of equipment.

Acknowledgement

Thanks for the supports from the project "Standards for Emerging Engineering Majors and Construction of Characteristic Teaching Experiment Platforms" [Civil Aviation Education Talent Programs in China, NO. MHJY2025036], the open project "Research on the Color Recognition and Appearance Defect Detection System for Solar Cells" [Key Laboratory of Solar Energy Technology Integration and Application Promotion in Sichuan Provincial Universities, Grant No. TYNSYS-2018-Y-06], the project "Research on SLAM for Intelligent Civil Aviation Transportation Robots Based on Stereo Vision" [Civil Aviation Flight University of China, Grant No. 25CAFUC04024], and the project "Design of a Single-Star Simulation System for Calibration of Aviation Attitude Determination Star Sensors" [Chengdu Aeronautic Industry and Cultural Development Research Center, Grant No. CAIACDRCXM2024-04].

References

[1] KARMIRIS-OBRATAŃSKI, P., PAPAZOGLOU, E.L., LESZCZYŃSKA-MADEJ, B., ZAGÓRSKI, K., MARKOPOULOS, A.P. (2021). A Comprehensive Study on Processing Ti-6Al-4V ELI with High Power EDM. *Materials*, Vol. 14, No. 2, pp. 303. https://doi.org/10.3390/ma14020303

[2] YANG, S., WANG, P., WANG, X. (2024). Comparative analysis between theoretical calculation and practical deformation of heavy forging hydraulic press (in Chinese). *China Metalforming Equipment & Manufacturing Technology*, Vol. 59, No. 2, pp. 18-25. https://doi.org/10.16316/j.issn.1672-0121.2024.02.003

[3] OTHMAN, S.M., SUNAR, N., ISMAIL, A.H., AYOB, M.N., AZMI, M.M., HASHIM, M.S.M. (2021). Position tracking performance with fine-tune Ziegler-Nichols PID controller for electro-hydraulic actuator in aerospace vehicle model. *Journal of Physics: Conference Series*, Vol. 2107, No. 1, pp. 012064. DOI 10.1088/1742-6596/2107/1/012064

[4] LIN, F., YAO, W., QIN, G.H., YE, H.C., TAO, J. (2021). Coupling effect of initial residual stress-initial geometric error on machining deformations of aeronautical monolithic components and its control. *Acta Armamentarii*, Vol. 42, No. 12, pp. 2731-2742. DOI: 10.3969/j.issn.1000-1093.2021.12.021

[5] LIM, E., HWANG, S.J. (2016). Modeling of the strut-and-Modeling of the strut-and-tie parameters of deep beams for shear strength prediction. *Engineering Structures*, Vol. 108, pp. 104-112. https://doi.org/10.1016/j.engstruct.2015.11.024

[6] ÇAKIROĞLU, R. (2022). Analysis of EDM machining parameters for keyway on Ti-6Al-4V alloy and modelling by artificial neural network and regression analysis methods. *Sādhanā*, Vol. 47, No. 3, pp. 150.https://doi.org/10.1007/s12046-022-01926-y

[7] LIU, Y.Y., XI, J.L., BAI, H.F., WANG, Z.N., SUN, L.L. (2021). A general robot inverse kinematics solution method based on improved PSO algorithm. *IEEE Access*, Vol. 9, pp. 32341-32350.DOI: 10.1109/ACCESS.2021.3059714

[8] WOLFGARTEN, M., RUDOLPH, F., HIRT, G. (2020). Analysis of process forces and geometrical correlations for open-die forging with superimposed manipulator displacements. *Journal of Materials Processing Technology*, Vol. 276, pp. 116408. https://doi.org/10.1016/j.jmatprotec.2019.116408

[9] WANG, Y.F., WANG, C., XU, Y.T., SUN, R., XIAO, K., WANG, K.L. (2024). A digital twin task scheduling method for intelligent manufacturing unit operations under edge-cloud collaboration (in Chinese). *Journal of Mechanical Engineering*, Vol. 60, No. 6, pp. 137-152. DOI: 10.3901/JME.2024.06.137

[10] ZHOU, Y.X., CHEN, Y., DENG, F., HU, X.H. (2024). Research on deformation control technology of large integral wall panel machining. *Tool Engineering*, Vol. 58, No. 3, pp. 102-106. DOI: 10.3969/j.issn.1000-7008.2024.03.017

[11] AVERSA, R., PETRESCU, R.V., AKASH, B., BUCINELL, R., CHEN, G., LI, S., PETRESCU, F.I. (2017). Kinematics and Forces to a New Model Forging Manipulator. *American Journal of Applied Sciences*, Vol. 14, No. 1, pp. 60-80. DOI: 10.3844/ajassp.2017.60.80

[12] LIN, F., YAO, W., QIN, G.H., YE, H.C., TAO, J. (2021). Coupling effect of initial residual stress-initial geometric error on machining deformations of aeronautical monolithic components and its control. *Acta Armamentarii*, Vol. 42, No. 12, pp. 2731-2742. DOI: 10.3969/j.issn.1000-1093.2021.12.021

[13] KE, S.T., DU, L.Y., GE, Y.J., TAMURA Y. (2018). Multi-dimensional wind vibration coefficients under suction for ultra-large cooling towers considering ventilation rates of louvers. *Structural engineering and mechanics: An international journal*, Vol. 66, No. 2, pp. 273-283. https://doi.org/10.12989/sem.2018.66.2.273

[14] WANG, G., HUANG, P. (2022). Innovative Design of a Hydraulic Press Mobile Station Based on TRIZ Theory. *Engineering Proceedings*, Vol. 24, No. 1, pp. 10. https://doi.org/10.3390/IECMA2022-12889

[15] AWAIS, M., SORVARI, J., TANNINEN, P., LEPPÄNEN, T. (2022). Finte element analysis of the press forming process. *International Journal of Mechanical Sciences*, Vol. 131-132, pp. 767-775. https://doi.org/10.1016/j.ijmecsci.2017.07.053

[16] ZEMANOVA, J., CABRNOCH, B., KRAL, M. (2026). Thermoplastic resin flow behaviour in foam core sandwich composites for aerospace applications during vacuum infusion process. *Manufacturing Technology*, Vol. 26, No. 2, pp. 249-256. https://doi.org/10.21062/mft.2026.018

[17] BREZNICKÁ, A., MIKUŠ, P., TIMÁROVÁ, Ľ., KOHUTIAR, M., KRBAŤA, M. (2024). Possibilities of analyzing sources of impurities in hydraulic oil. *Manufacturing Technology*, Vol. 24, No. 5, pp. 721-730. https://doi.org/10.21062/mft.2024.081

[18] XU, W., ZHAO, X., SHI, H., HUANG, L. (2025). Study on trapped oil and cavitation of jet fuel gear pump. *Manufacturing Technology*, Vol. 25, No. 1, pp. 131-142. https://doi.org/10.21062/mft.2025.005